Quantum Electronics **42** (11) 964–979 (2012)

INVITED PAPER

PACS numbers: 42.55.Wd; 42.55.Px; 42.55.Ye; 42.65.Dr; 42.60.Da; 42.60.Fc
DOI: 10.1070/QE2012v042n11ABEH014946

Nonlinear fibre-optic devices pumped by semiconductor disk lasers

A.Yu. Chamorovskiy, O.G. Okhotnikov

Abstract. **Semiconductor disk lasers offer a unique combination of characteristics that are particularly attractive for pumping Raman lasers and amplifiers. The advantages of disk lasers include a low relative noise intensity (–150 dB Hz^{-1}), scalable (on the order of several watts) output power, and nearly diffraction-limited beam quality resulting in a high (~70%–90%) coupling efficiency into a single-mode fibre. Using this technology, low-noise fibre Raman amplifiers operating at 1.3 μm in co-propagation configuration are developed. A hybrid Raman-bismuth doped fibre amplifier is proposed to further increase the pump conversion efficiency. The possibility of fabricating mode-locked picosecond fibre lasers operating under both normal and anomalous dispersion is shown experimentally. We demonstrate the operation of 1.38-μm and 1.6-μm passively mode-locked Raman fibre lasers pumped by 1.29-μm and 1.48-μm semiconductor disk lasers and producing 1.97- and 2.7-ps pulses, respectively. Using a picosecond semiconductor disk laser amplified with an ytterbium-erbium fibre amplifier, the supercontinuum generation spanning from 1.35 μm to 2 μm is achieved with an average power of 3.5 W.**

Keywords: *semiconductor disk laser, fibre lasers and amplifiers, semiconductor saturable absorber mirror, ultrashort pulses, stimulated Raman scattering, supercontinuum generation.*

1. Introduction

Efficient operation of nonlinear fibre-optic devices is critically dependent on the pump power density. Fibre lasers and amplifiers based on the stimulated Raman scattering are the most important and widespread examples of the optical sources exploiting nonlinear-optical effects. They are essentially core-pumped devices because the power density inside a fibre core is the parameter that determines nonlinear conversion efficiency.

In this review we demonstrate the advantages of semiconductor disk lasers, also known as vertical-external-cavity surface-emitting lasers, for pumping fibre Raman oscillators. These lasers can generate multiwatt powers with diffraction-limited beam quality which allows for high efficient light coupling into the core of single-mode fibres, compared to other types of semiconductor solid-state lasers [1]. In addition, flexible wavelength versatility inherent in semiconductor materials combined with superior noise properties of disk lasers provide a promising platform for creation of advanced fibre-optical amplifiers. Throughout this study we demonstrate experimentally the advantages of applications of semiconductor disk laser for pumping low-noise amplifiers, continuous-wave and passively mode-locked Raman fibre lasers. The results of the experiments on generation of picosecond pulses using passively mode-locked Raman fibre lasers are presented and the possibility of creating an oscillator with an ultrawide tuning range based on a picosecond semiconductor disk laser is discussed.

A.Yu. Chamorovskiy, O.G. Okhotnikov Optoelectronics Research Centre, Tampere University of Technology, Finland, P.O. Box 692, FIN 33101; e-mail: alexander.chamorovskiy@tut.fi

Received 11 July 2012
Kvantovaya Elektronika **42** (11) 964–979 (2012)
Translated by A.Yu. Chamorovskiy

2. Fibre Raman oscillators

The effect of Raman scattering was first observed by Mandelstam and Landsberg in 1928 during the study of optical properties of the crystals [2]. The same effect was simultaneously found in liquids by Krishnan and Raman [3]. Stimulated Raman scattering was first reported in 1964 while investigating the performance of the ruby laser [4]. First observation of the stimulated Raman scattering in optical fibres was described by Stolen and Ippen in 1973 [5].

Rapid development of the fibre optics in the 1980s revealed unique features of Raman scattering [6]. Mollenauer et al. proposed the Raman amplification for ultrashort pulse generation in 1984 [7]. In 1986 Stolen et al. reported the first demonstration of data transmission in a fibre link using Raman amplification [8]. Relatively broad Raman gain bandwidth in silica of about 5 THz can support the femtosecond pulse generation, while the spectral band of Raman amplification depends on the pump wavelength, which makes it possible to develop laser systems emitting at different wavelengths.

The rare-earth doped fibre amplifiers start to dominate at the end of 1980s owing to the tremendous progress in technology of doped silica fibres. Raman fibre lasers and amplifiers require relatively high levels of pump power due to the low gain – tens of milliwatts per every dB of amplification, whereas for rare-earth erbium fibre amplifiers this value is few tenth of a milliwatt per dB [6]. It should be noted that pumping of Raman devices requires the sources operating at specific wavelengths which calls for additional technological efforts. Meanwhile, ytterbium (Yb), erbium (Er) and thulium (Tm) fibre oscillators have become commercially successful products in less than a decade.

The renewal of interest in Raman devices started at the early 1990s when high power semiconductor and fibre pump sources became commercially available [9–11]. Currently, fibre Raman amplifiers are widely used in fibre-optic com-

munication networks [12, 13]. Raman devices ensure less noise and nonlinear disturbances to the transmitted signal compared to erbium amplifiers [14]. Nowadays, Raman amplifiers are employed in the most long-haul (over 300 km) fibre data networks [15]. Further development of fibre Raman oscillators became possible also due to the remarkable progress in fibre technology, which led to a substantial improvement in silica fibre quality. As a consequence, the Raman laser threshold was decreased by several orders of magnitude – from hundreds of watts to hundreds of milliwatts [16]. The progress in fibre Bragg grating technology allows all-fibre Raman devices and multi-cascade Raman convertors to be built [17].

Raman lasers could also be used as pump sources for other types of optical oscillators, e.g. erbium and thulium fibre lasers [16, 18]. They are also used in second-harmonic generation and other types of nonlinear optic devices [19, 20] and find application in metrology and space communications [21]. The primarily advantage of Raman lasers is capability to generate a signal virtually at any wavelength within the transparency window of optical fibre, these wavelengths being unavailable for rare-earth or semiconductor light sources. Under certain conditions, the maximum efficiency of Raman conversion is reported to reach to date ~84.2% [22].

As mentioned above, the high conversion efficiency assumes direct pumping into the fibre core and, therefore, requires single transverse-mode pump sources. The experiments with cladding-pumped Raman devices using the geometry similar to double-clad rare-earth fibre lasers demonstrated low efficiency, though 100 W of output power at 1120 nm was obtained using multimode ytterbium fibre pump source [23]. However, the generation efficiency of a Raman signal was rather low compared to the case of single-mode pumping [24, 25]. Moreover, the beam quality of the double-clad fibre Raman laser exhibits the degradation with the increase in the pump power. Thus, there is a need for high power single mode pump sources for efficient light coupling into the core of nonlinear fibres. Raman amplifiers require typically hundreds of milliwatts of pump, while the pump power for high power Raman lasers is on the level of tens of watts. Since Raman amplification exhibits high pump-to-signal noise conversion, the pump source should generate the low noise output [26].

2.1. .Stimulated Raman scattering in optical fibres

Amplification utilising the Raman effect can be obtained over the whole transparency window of silica optical fibres ranging from 0.3 to 2.2 μm provided that the suitable pump source is available [27, 28]. In this case, the lasing wavelength directly depends on the pump wavelegnt. The Raman gain peak is determined by the optical phonon frequency and the pump wavelength (Fig. 1a) [13, 19]. The Raman gain in the optical fibre in the small-signal approximation can be described using the expression [13]:

$$G_R = \exp\left(\frac{g_R P_0 L_{eff}}{k A_{eff}}\right). \quad (1)$$

Here P_0 is the pump power; g_R is the Raman gain for the given medium ($g_R \approx 10^{-13}$ m W^{-1} for silica); L_{eff} is the effective interaction length; A_{eff} is the effective mode field area in the optical waveguide; and k is the factor depending on the pump and signal polarisations, ($k = 2$ for random-polarised beams). The Raman gain features a relatively flat spectrum with a broad gain bandwidth of almost 5 THz (Fig. 1b) [13]. Implementation of several pump sources with different wavelengths allows for further extension of the gain bandwidth and enables the control of the gain flatness. The Raman gain is independent of the relative directions of pump and signal propagation in the cavity, which provides notable flexibility in designing Raman lasers and amplifiers of different configurations with desirable parameters [15]. The Raman gain, however, is very sensitive to the relative polarisations of the pump and signal, and the most efficient pump-to-Raman signal conversion occurs for identical polarisation states [29]. Therefore, accurate control of the polarisation state is required for both pumping the source and Raman laser cavity.

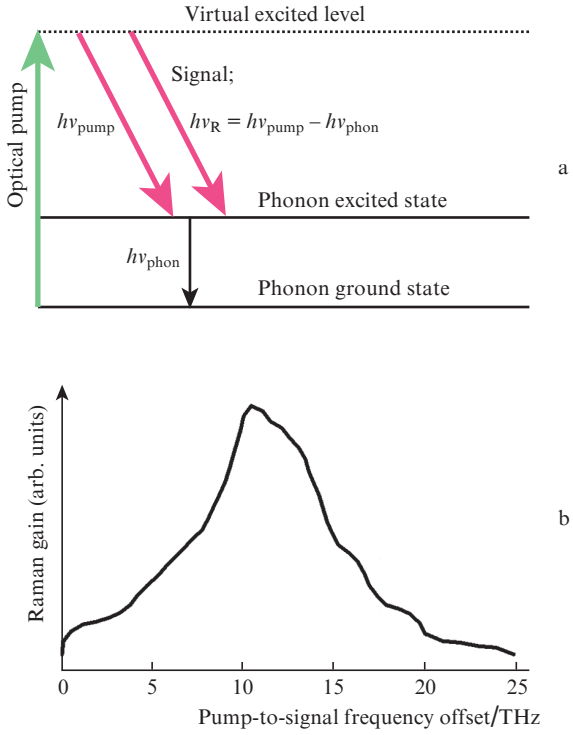

Figure 1. (a) Stimulated Raman scattering in optical fibres and (b) Raman gain spectrum in silica.

The femtosecond response of the Raman scattering process results in a strong noise transfer from pump to signal [30]. In order to minimise this detrimental effect in Raman amplifiers regularly pumped with inexpensive noisy diode lasers, the counterpropagation configuration is employed using opposite propagations of the pump and signal [15]. This configuration, however, could not take full advantage of Raman amplification technology.

2.2. Raman fibre amplifiers

The characteristics of the pump source for a fibre Raman amplifier is of great importance since pump fluctuations would be instantly transferred to the amplified signal and thus deteriorate the noise figure of the system (NF). The resulting relative intensity noise (RIN) of the signal could be even higher than that of the pump source. However, if the pump and signal interaction length is relatively long (several kilometres and more), the efficient noise averaging and even

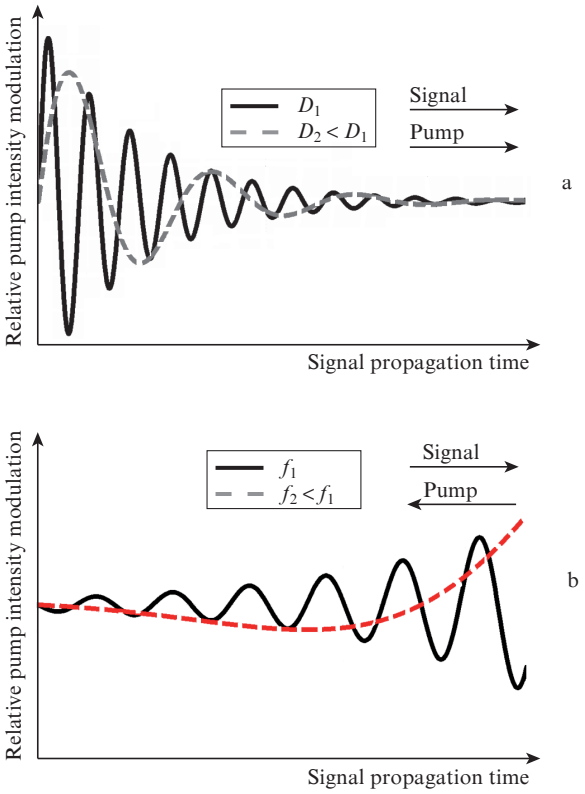

Figure 2. Pump fluctuations experienced by the signal in the case of (a) copropagation with different chromatic dispersions D_1 and D_2 ($D_1 > D_2$) (the fluctuation frequency is constant) and (b) counterpropagation with different pump fluctuation frequencies f_1 and f_2 ($f_1 > f_2$) [26].

suppression could occur (Fig. 2). The impact of this phenomenon is dependent on the relative propagation directions of the pump and signal [26].

In counterpropagation configuration the pump fluctuations would suffer the effect of low-pass band filtering. High-frequency noise (from few MHz and higher) would be efficiently averaged due to the delay between the pump and signal and the long interaction length. Consequently, the corresponding fast Raman gain fluctuations would be also averaged. In this case, low-frequency gain fluctuations (on the order of kHz) would induce slow fluctuations in the effective Raman gain, which would be further transferred to the amplified signal. When the gain fluctuation period τ_{fl} is larger than the propagation time of the signal along the given distance L_{eff},

$$\tau_{fl} \geqslant nL_{eff}/c \qquad (2)$$

(here n is the refractive index of the medium and c is the speed of light), the efficient pump noise averaging would occur even at low frequencies [13, 26, 31].

In the case of copropagation configuration, noise averaging would occur due to the group velocity difference between the pump and the signal caused by the chromatic dispersion in the optical fibre. The higher the chromatic dispersion of the fibre, the stronger the noise averaging. In this case, the averaging efficiency apparently increases with increasing fluctuation frequency. This scenario is demonstrated in Fig. 2.

The pump noise level requirements in modern communication networks depend essentially on the Raman amplifier configuration. For a counterpropagation scheme, the RIN level of the pump source should be lower than –90 dB Hz^{-1}, whereas in a copropagating setup this value should be better than –20 dB Hz^{-1} [15, 32]. The counterpropagation configuration is preferential today in practical communication system because of relaxing requirements for the noise of the pump sources. Copropagating amplifiers, however, could offer a higher efficiency of pump conversion and require a lower intensity of the input signal and provide better performance of broadband discrete Raman amplifiers [31, 33]. Of practical importance is the fact that they allow one to reduce the operation costs because of an increased span between concatenated amplifiers in long-haul transmission lines [34]. In order to practically implement this configuration, however, the low-noise single mode pump sources are required.

2.3. Mode-locked Raman fibre lasers

Raman sources are of interest for generation of short and ultrashort pulses. Broad gain bandwidth and fast response time enable the Raman scattering mechanism to support femtosecond-pulse generation [35]. However, state-of-the-art mode-locked fibre lasers using rare-earth doped glasses as a gain medium demonstrate better performance than ultrashort fibre Raman lasers [36–41].

The overview of experimental results for mode-locked fibre Raman lasers is presented in Table 1. The authors of [37] describe passive mode-locking in a fibre ring resonator using dissipative four-wave mixing and spectral mode selection by a specially designed fibre Bragg grating. The laser generated 600-fs pulses with an average power of 400 mW and high repetition rate of 100 GHz, which resulted in a relatively low pulse energy of 0.04 nJ. Mode-locking with an amplifying loop mirror in the figure-of-8 cavity was demonstrated by Chestnut et al. [38]. An all-fibre laser cavity combined with Raman amplification suitable for operation in a broad spectral range enables pulse generation at various wavelengths – 1.33, 1.41, and 1.57 μm. The pulse duration was varied in the range of 440–860 fs. Unfortunately, the laser exhibited low efficiency (for a 5.2 W of the pump power the average output power was only 10 mW) and high sensitivity to external fluctuations. A short-pulse fibre ring Raman laser with an active erbium-doped loop mirror acting as a saturable absorber and continuous-wave fibre Raman laser as a pump source has been recently demonstrated [39]. Parabolic-shape pulses with duration of 6 ps and energy of 22 nJ at the central wavelength of 1534 nm have been obtained. Implementation of the rare-earth saturable absorber in this design, however, limits the operation bandwidth of the laser. Mode-locking in Raman lasers has been recently reported using saturable absorbers based on carbon nanotubes and graphene exhibiting broadband nonlinear response [40–43]. The pulses with duration below 2 ps and energy of 3 nJ were obtained at 1665 nm and 1550 nm with carbon nanotubes and graphene absorbers, respectively. Efficiency of these lasers was still low – the output power was about 10 mW for several watts of the launched pump power.

It should be noted that most demonstrations use a cw fibre Raman laser as pump source, which indicates the shortage of other types of single-mode pump lasers with the required output characteristics. Using cascaded Raman fibre lasers pumped by rare-earth fibre lasers as sources of optical pumping involves, however, much complexity in Raman-based systems.

Table 1. Experimental results obtained for passively mode-locked fibre Raman lasers.

Laser configuration	Pump source type	Length and nonlinear coefficient γ	Operating wavelength/nm	Shortest pulse duration	Average power and repetition rate	References
Ring cavity with dissipative four wave mixing	CW Raman laser, 1450 nm, 4.5 W	1 km, 14 W^{-1} km^{-1}	1550	600 fs	430 mW, 100 GHz	[37]
Figure-of-8 laser cavity	CW Raman laser, 1257 nm, 5.2 W 1316 nm, 5 W 1455 nm, 3.1 W	2–4.5 km, 0.9 W^{-1} km^{-1}	1330 1410 1570	500 fs 860 fs 440 fs	10 mW 1 mW	[38]
Ring cavity with Er-doped amplifying loop mirror	CW Raman laser, 1435 nm, 1.5 W	2.4 km, 5.7 W^{-1} km^{-1}	1534	6 ps	1.25 mW, 64 kHz	[39]
Ring cavity with a carbon nanotube saturable absorber	CW erbium-doped fibre laser,1555 nm, 15 W	100 m, 2.5 W^{-1} km^{-1}	1665	2 ps	5 mW	[40]
Ring cavity with a 4-layer graphene saturable absorber	CW Raman laser, 1450 nm, 5 W	100–200 m, 2.5 W^{-1} km^{-1}	1550	350 ps	8.5 mW, 332.5 MHz	[41]

2.4. Pump sources for fibre Raman oscillators

To date, the main sources for pumping Raman devices are semiconductor diodes and fibre lasers. Single-mode diode lasers operating in 900–980-nm and 1400–1500-nm spectral ranges are the most popular pump sources for erbium-doped fibre amplifiers, which are widely used to transmit information in modern optical communication networks in the 1.55-μm spectral region [32]. The output power up to ~800 mW launched into a single-mode fibre at the wavelength of 980 nm is commercially available [44]. This power is sufficient for pumping a Raman amplifier, though the lasers using this gain mechanism require watt levels of pump power. The Bragg grating wavelength-stabilised semiconductor diodes used broadly for pumping erbium fibre amplifiers have a typical RIN value of –100 dB Hz^{-1}, which limits the performance of Raman amplifiers and lasers [32]. Fabry–Perot narrow-line laser diodes can offer a low RIN, but require accurate thermal and current control to avoid the spectral variations [45]. A relatively novel type of laser diodes – inner grating multimode (iGM) diodes [46], exhibit a low RIN value of –140 dB Hz^{-1} and produce the output powers over 300 mW [47]. These devices, however, are still under extensive investigation and available to date only for the 1470–1520-nm spectral range.

Fibre lasers are capable of delivering high powers in the single-mode regime and used for optical pumping of Raman systems [48]. Thus, Yb-doped single-mode cw fibre lasers with an output power over 10 kW have recently been demonstrated [49]. Single-mode Tm-doped fibre lasers with an output power up to 300 W are available now [50] and cw Er-doped systems could produce the power in the range of 10–100 W [51]. Nevertheless, the operating wavelength of rare-earth doped fibre sources is limited to spectral bands at 1, 1.55, and 1.9 μm depending on the active dopant. Active ions with a broadband gain spectrum, e.g. bismuth (Bi) doped fibre, are still at early stage of development [52].

A typically high RIN value of fibre lasers needs to be carefully addressed when they are used as pump sources, which is due to the comparably high noise level appearing because of the high density of amplified spontaneous emission (ASE) [53, 54]. In particular, cascaded amplification combined with stimulated Brillouin scattering (SBS) is implemented to overcome excessive noises of the fibre lasers. The amplifier enables the efficient pump conversion and high output powers, whereas the SRS effectively narrows the gain bandwidth [53]. Devices based on this principle typically operate in the spectral range of 1030–1064 nm and 1520–1570 nm. It should be noted that the SBS gain has a bandwidth of only tens of MHz, and the Stokes frequency shift depends on the thermal and environmental perturbations and, therefore, the system requires a complex stabilisation techniques [54, 55].

In order to further extend the spectral range, cascaded Raman amplification using a high power fibre laser pump is typically implemented. The two-stage amplification was demonstrated in phosphate fibre (1.06 μm → 1.24 μm → 1.48 μm) with the overall conversion efficiency of 40% [56]. For a silica fibre the two-stage amplification (1.06 μm → 1.23 μm → 1.3 μm), the efficiency was in the range of 46% [57]. Using cascaded Raman amplification it is virtually possible to generate the signal at any wavelength within the whole transparency window of the silica fibres [58].

Fibre lasers acting as a pump source for Raman oscillators have a number of shortcomings. First, the overall efficiency of the multistage Raman amplification decreases with every successive Stokes shift. Secondly, it requires various intracavity elements, like fibre Bragg gratings, to be implemented and they should sustain considerable intracavity powers. Moreover, waveguiding properties of the fibre tend to deteriorate when operating considerably far from a cutoff wavelength [59]. Since the Raman conversion efficiency increases with increasing fibre length, the threshold of nonlinear effects, e.g. SBS, decreases, which can deteriorate the overall performance of the cascaded generator. Finally, implementation of an efficient short-pulse laser based on multistage Raman amplification is a laborious task [60]. Further progress of the Raman fibre oscillators requires advanced types of pump sources which would combine the wavelength versatility inherent in semiconductor gain media and high output powers with diffraction-limited beam quality typical of solid-state and fibre lasers.

3. Semiconductor disk lasers for pumping fibre Raman oscillators

This study considers the potential of semiconductor disk lasers (SDLs also known as VECSELs) as pump sources for Raman and other nonlinear-optic fibre devices [61]. SDLs can produce a circular diffraction-limited high-power beam owing to an extended vertical cavity and suppressed thermal lens effect. The SDL cavity allows different intracavity elements, like nonlinear crystals, bandpass filters or saturable absorbers to be easily integrated. Though the SDLs could be pumped by current injection or optically, this study is focused entirely on optically pumped SDLs because this pumping approach has a large potential for power scaling, which is a primary objective in nonlinear-optic applications. The SDL wavelength can be tailored over a wide range by varying the composition of the gain medium, similar to other types of semiconductor sources. The broad gain band of the semiconductor active medium makes it possible to pump this medium by conventional multi-mode laser diodes, and the small length of the active element facilitates the focusing of the pump.

3.1. Semiconductor disk lasers

The thin-disk laser concept was invented primarily as a means to suppress the beam distortion due to the thermal lens effect [62]. The SDL structure is similar to the solid-state disk laser geometry except for the semiconductor gain medium used instead of a crystal or glass material and exhibiting a gain several orders of magnitude higher [63].

The schematic of a typical SDL is shown in Fig.3. A typical gain element of the SDL comprises a semiconductor gain medium with a number of quantum-well or quantum-dot layers sandwiched between barrier layers, usually acting as pump absorbing media. The structure is usually monolithically grown together with a distributed Bragg reflector and conveniently allows one to use the gain element in a cavity in the reflection regime. The cap layer (transparent both for the pump and signal) grown on top of the quantum confined gain medium provides electron confinement and suppresses diffusion of excited carriers to the surface and their consequent nonradiative recombination [1]. Since the SDL operates with a considerable thermal load of the gain medium, the efficient heat removal is a critical feature for achieving high output powers. The active element is bonded on the heat spreader; moreover, an additional intracavity transparent heat spreader placed on top of the structure is frequently used to further enhance the heat removal.

The original idea of a semiconductor active mirror – the key element of an SDL, was proposed by N.G. Basov in his Nobel lecture in 1964 [64, 65]. First experimental demonstration of an SDL as an extended format of vertical cavity semiconductor lasers was made by Jiang et al. in 1991 [66]. The semiconductor gain medium made of InGaAs quantum wells was placed on a gold mirror forming a reflector with a built-in gain. This laser emitted about 400 mW at the wavelength of 1.5 μm. The next year same authors proposed the design with the distributed Bragg reflector used instead of the metal mirror [67]. In 1997, Kuznetsov et al. [68] demonstrated an SDL producing 700 mW of output at the wavelength of 1 μm. This study formed the current concept of a diode-pumped SDL, discussed various types of cavities and the potential for power scaling. Table 2 summarises the achievements of modern SDLs operating at different wavelengths reported to date.

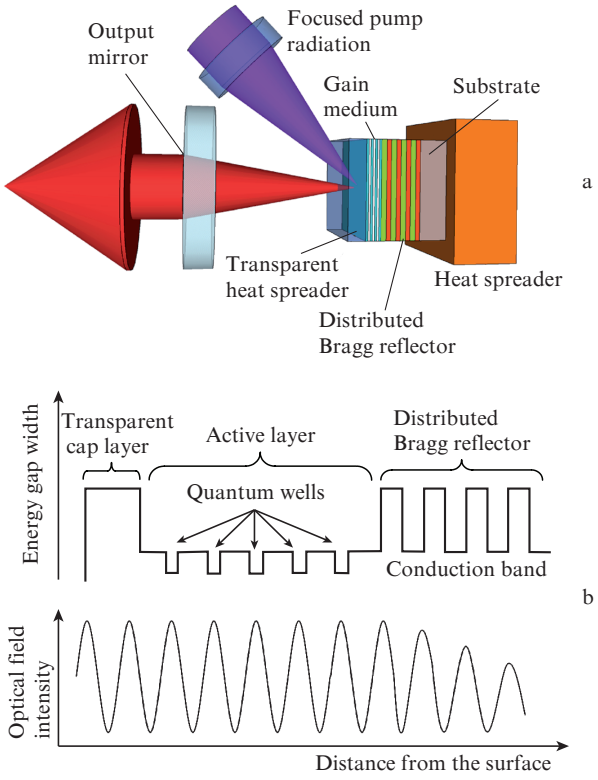

Figure 3. (a) Schematic of an SDL and (b) conduction band and the structure of the semiconductor gain mirror and the corresponding optical field intensity distribution.

Table 2. Parameters of various SDLs operating at different wavelengths.

Pump wavelength/nm	Lasing wavelength/nm	Gain medium	References
532	674	GaInP	[69]
822	853	GaAs	[70]
800–808	920–1060	InGaAs	[71–73]
788–800	1180–1220	InGaAsN	[74, 75]
980	1300	AlGaInAs	[76]
980	1480–1570	AlGaInAs	[77, 78]
980	2005	GaInSb	[79]
1960	2350	GaInAsSb	[80]

Currently, single-mode SDLs with a high quality of the output beam are demonstrated over the whole transparency window of silica fibres. Further tailoring to the short wavelengths is performed by frequency doubling [81]. The high Q-factor of the SDL cavity allows for considerable energy storage and, consequently, enhances substantially the intracavity nonlinear conversion.

Figure 4a presents the output powers of different single-mode SDLs reported to date. The high quality of the output beam intrinsic to this class of lasers allows reaching up to 90% coupling efficiency inside the single-mode fibre, as can be seen from Fig.4b [82, 83]. Although, both injection [83, 87–90] and optical [1] pump techniques can be applied to SDL excitation, currently only optically pumped SDLs are capable of producing multi-watt output powers. The development of electrically pumped SDLs, however, demonstrates sensible progress [91]. Some experimental results on the SDLs with an injection pumping reported to date are presented in Table 3.

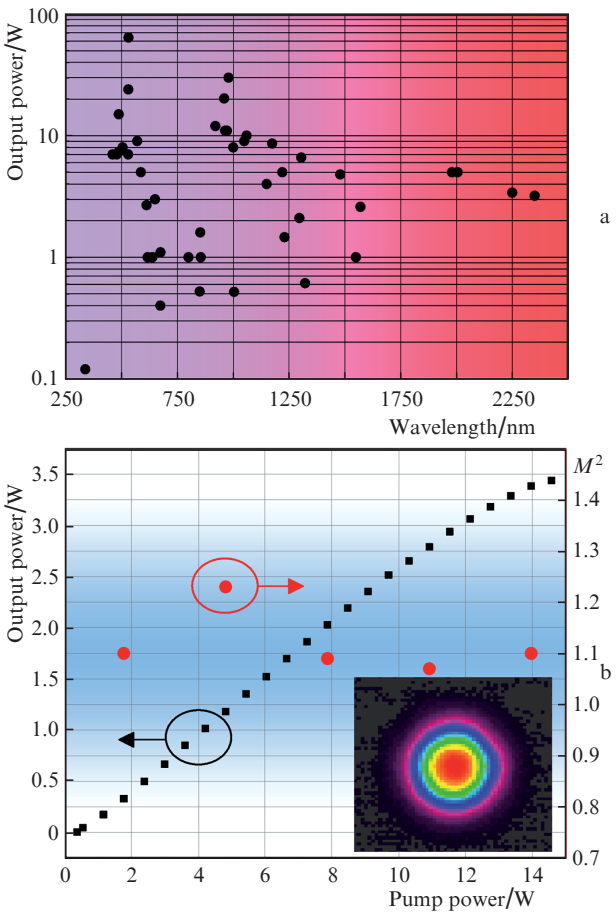

Figure 4. (a) Output powers of the single-transverse-mode SDLs operating at various wavelengths. Data are borrowed from [1, 78, 84–86] and (b) output power and the beam quality parameter M^2 vs. the optical pump power for a 1-μm single-mode SDL. Inset: SDL output beam profile image.

Table 3. Characteristics (reported to date) of modern electrically pumped SDLs.

Lasing wavelength/nm	Output power/mW	References
485	1.7	[87]
490	40	[83]
974	50	[87]
980	500	[83, 88]
1520–1540	0.12	[89]
1540	2.7	[90]

3.2. SDLs for pumping fibre Raman amplifiers

Noise characteristics of the pump source may limit essentially the performance of the fibre Raman amplifier. From this perspective, it is of imperative importance that SDLs could operate with RIN values limited to the shot noise level [92, 93], which is significantly better than the requirements imposed by the communications industry [15, 32]. In 2008 Baili et al. [92] demonstrated a 1-μm SDL with the cavity length less than 50 mm that exhibited shot noise limited RIN value of –155 dB Hz^{-1} for the photocurrent of 1 mA in the frequency range spanning from 50 MHz to 18 GHz. The analysis suggests that the shot noise limited operation is expected when the photon lifetime in the cavity is longer than the carrier lifetime due to the high Q-factor and/or the short cavity length. The photon lifetime τ_{ph} is determined by the cavity round-trip time τ_{pass} and the loss per round-trip α [94]:

$$\tau_{ph} \sim \tau_{pass}/\alpha. \quad (3)$$

For a 45-mm-long cavity and passive loss per round-trip of 1.5% the photon lifetime would be 20 ns, which is considerably longer than the carrier lifetime before recombination (in the range of a nanosecond). The laser operation in this regime, also known as the A-class noise regime, exhibits uniform and flat spectral noise density and suppressed perturbations caused by the relaxation oscillations. In addition, the low frequency RIN reduction in the range of 45 kHz – 50 MHz was obtained by minimising the cavity loss and applying the electronic noise suppression system to the pump diode. Pal et al. [93] proposed RIN suppression using a specially designed InGaAs/GaAsP gain structure and experimentally demonstrated a low noise dual frequency SDL.

In this study we report the fibre Raman amplifiers operating in the 1.3-μm spectral range pumped by a 1.22-μm SDL. This wavelength range, also known as O-band, is of the special interest since standard optical fibres have here a zero dispersion wavelength and, therefore, the chromatic distortions are greatly reduced [95]. The development of fibre networks operating in this spectral region suffers from the shortage of efficient fibre amplifiers. Nd, Yb, Er, and Tm-doped fibres are unable to provide a sufficient gain at 1.3 μm. Though chalogenide praseodymium-doped fibres could provide an amplification in the wavelength range of 1290–1340 nm, they offer relatively low efficiency [96, 97] and have obstacles in coupling with silica-based fibres. Thus low-noise fibre Raman amplifiers based on silica fibres are attractive candidates for O-band fibre communication networks [48, 98, 99].

3.2.1. 1.3-μm fibre Raman amplifier pumped by a semiconductor disk laser. The single transverse mode 1.22-μm SDL used here as a pump source of a fibre Raman amplifier produced up to 1.8 W of linearly polarised output in a single-mode fibre corresponding to the coupling efficiency of 75%. The SDL was pumped with a fibre coupled multimode diode laser operating at 808 nm. Schematic of the 55 mm-long SDL cavity is shown in Fig. 5.

The gain elements for high-power operation in the 1.2–1.5-μm spectral range are normally based on GaInNAs materials, or employ the wafer fusion technique which allows

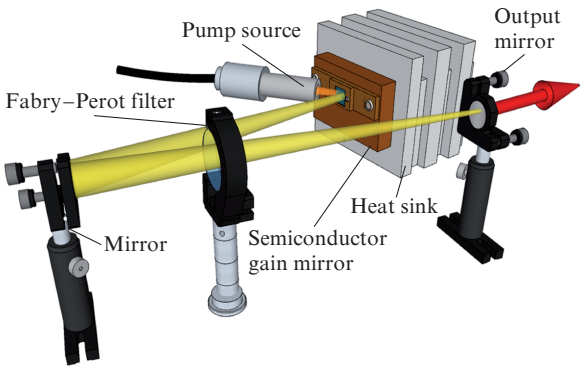

Figure 5. Schematic of the V-cavity SDL operating at 1.22 μm. The number of the longitudinal modes and overall laser performance was stabilised with an intracavity Fabry–Perot filter.

one to create a monolithic gain mirror by integrating semiconductor materials with large difference in the lattice constant [74, 100, 101]. The semiconductor gain mirror used in this study was made of a GaInNAs material grown on a GaAs substrate using molecular beam epitaxy (MBE). The gain structure was comprised of 30 pairs of 10 GaInNAs quantum wells of thickness 7 nm. The distributed Bragg reflector was made of 30 GaAs/AlAs layers. The transparent $Al_{0.37}Ga_{0.63}As$ cap layer was placed on top of the gain medium to prevent nonradiative carrier recombination from the gain mirror surface. The gain mirror was then placed on a heat sink and the temperature of the sample was kept at 15°C.

The RIN value of the laser sources used in the experiment was calculated according to the method, which is described in detail in [102]. The RIN values can be estimated using the signal spectral density $S_{sp}(\omega)$, photodetector sensitivity R, and the signal optical power P:

$$\mathrm{RIN} = \frac{S_{sp}(\omega)}{R^2 P^2}. \quad (4)$$

Measurements were carried out using a photodetector with a 3-GHz bandwidth. The minimal RIN value limited by the shot noise was estimated to be –160 dB Hz^{-1} for a 0.5-mW optical signal. Optical attenuation of the detected signal was applied at high output powers of the devices under test. The error in the RIN measurements RIN_{err} due to limited quantum efficiency of the photodetector was estimated using the relation [102]:

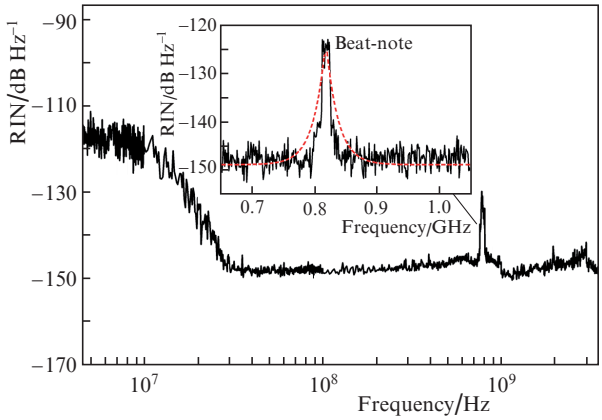

Figure 6. RIN measurements of the 800-mW, 1.22-μm SDL in the spectral window ranging from 1 MHz to 3 GHz. Inset demonstrates the intensity peak around 800 MHz, which is related to the frequency of longitudinal eigenmode beatings and noises caused by amplified spontaneous luminescence. This assumption is further confirmed with the well-fitted Lorentzian approximation (dashed line). The increase in the noise level is detected around this peak thus demonstrating the absence of the excessive noise [92].

$$\mathrm{RIN}_{err} = \frac{2q}{RP} + \frac{k_B T(F_a G_d + F_{sa} - 1)/G_d}{R^2 P^2} + \frac{4k_B T/R_{load}}{R^2 P^2}. \quad (5)$$

Here q is the electron charge; k_B is the Boltzmann constant; T is the temperature; F_a, G_d, F_{sa} are the noise figures (NFs) of preamplifier, photodetector, and spectrum analyser, respectively; and R_{load} = 50 Ω. The calculations revealed that the error was in the range of 4%–6%.

Figure 6 demonstrates results of RIN measurements for a 1.22-μm SDL for the frequency range from 1 MHz to 3 GHz and power level of 800 mW. The RIN value was better than –150 dB Hz^{-1} in the broad spectral band except for the low frequency range where the pump diode and environmental fluctuations prevail. The noise peaks originated from relaxation oscillations have not been detected, demonstrating a uniform noise profile. The frequency component around 800 MHz corresponds to the longitudinal mode beating. The noise measurements clearly indicate that the low RIN value even at high powers is an intrinsic feature of the SDLs.

The 1.22-μm SDL in question was then used as a pump source for a fibre Raman amplifier with an experimental setup (Fig. 7) [99]. The amplifier is operated in the regime of the pump and signal copropagation. A 900-m-long highly nonlinear GeO_2-codoped silica fibre had a core doped with 25% molar concentration of GeO_2, core/cladding refractive index difference Δn = 0.03, numerical aperture NA = 0.25, and Raman gain 21 dB km^{-1} W^{-1}. The effective mode area at the wavelength of 1.3 μm was estimated to be 9 μm^2. Due to effective draining of the fibre perform, passive losses around 1.3 μm were below 2.2 dB km^{-1}. An optical isolator was used to prevent lasing in the amplifier. The pump and the signal were multiplexed and demultiplexed using 1.22/1.3-μm fibre multiplexers. The polarisation controllers stabilised the operation due to the polarisation sensitivity of the SRS. The multiplexer at the output was installed to couple out the unabsorbed pump.

As a reference signal source in the experiments, use was made of a 1.29-μm low power single-mode SDL. The fundamental frequency of the laser cavity was 21.5 GHz, and the measured RIN value before the amplification was –151 dB Hz^{-1} at the output level of 25 mW.

Figure 8 demonstrates the measured operation characteristics of the fibre Raman amplifier with an SDL pump. An amplification of 9 dB was achieved for an input signal of 2 mW, whereas the residual pump power filtered out by a fibre dichroic coupler was ~150 mW for the highest gain. Noise characteristics plotted in Fig.8 b were measured for 7–8-dB gain at the pump of 1.1 W. The RIN increase in the frequency range from 50 MHz to 3 GHz was below 2.3 dB which corresponds to the excessive noise of the Raman amplifiers with the counterpropagation configuration [103]. The RIN increase for frequencies below 50 MHz originates from

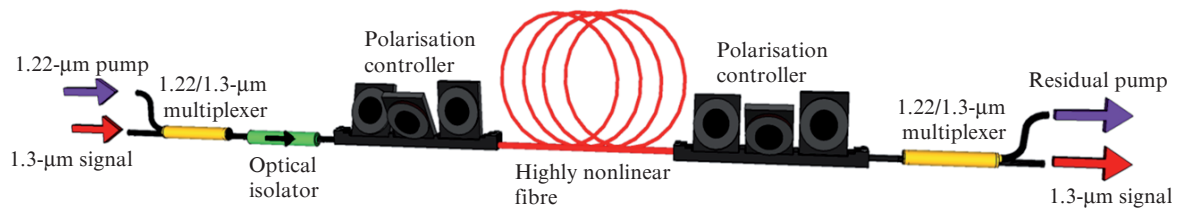

Figure 7. Schematic of the Raman fibre amplifier in the copropagating configuration.

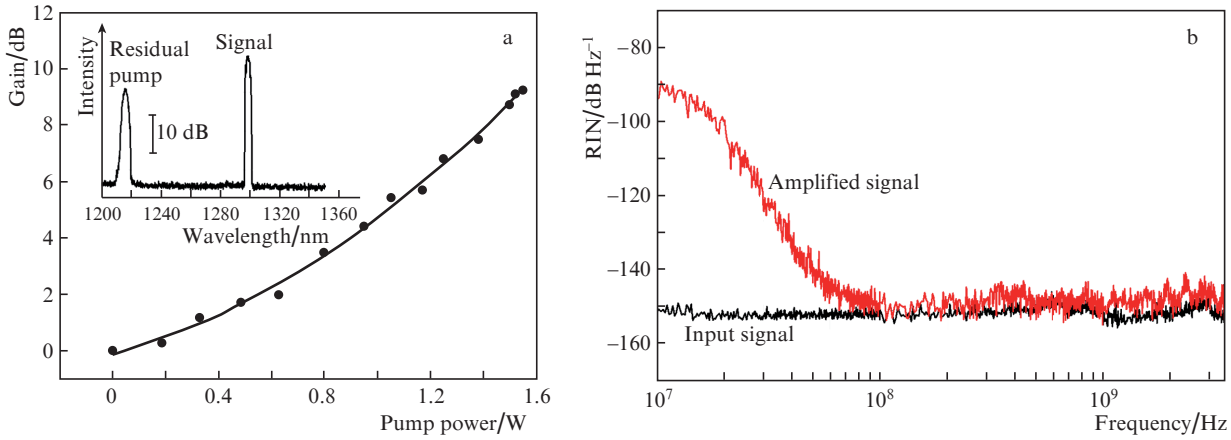

Figure 8. Performance of the Raman fibre amplifier pumped by SDL: (a) small signal gain vs. SDL pump power, inset demonstrates the amplifier output spectrum; (b) reference signal RIN measurements before and after the amplification. Optical power at the photodetector was 600 μW corresponding to the shot noise limit of –157 dB Hz^{-1}.

pump-to-signal noise transfer typical of Raman amplifiers operating in copropagating configuration. Regardless of these fluctuations induced by environmental perturbations, the RIN level at the low frequency range is below –90 dB Hz^{-1}. This value is still superior to the typical characteristics of the diode and fibre lasers operating at the similar power levels [15, 104]. For copropagating amplifier configuration, the low frequency perturbations can be efficiently suppressed by using the feedback circuit modulating the pump radiation in anti-phase with the fluctuations or some other noise suppression methods [105, 106]. The measured characteristics allow one to conclude that the SDLs operating in the 1.22–1.25-μm spectral region meet the telecommunication requirements for pumping O-band amplifiers. Next we will discuss other configurations of Raman amplifiers and, particularly, propose the 'hybrid' design for further improvements of the amplifier performance.

3.2.2. 1.3-μm hybrid Raman fibre amplifier pumped by an SDL. In the 1.3-μm fibre Raman amplifier described above more than 10% of the pump power remained unconverted. This feature, typical of discrete Raman amplifiers, deteriorates the overall system efficiency [107–109]. There are several methods for improving the pump conversion of discrete amplifiers. Nicholson et al. [107] proposed the combination of Bragg reflectors and metal mirrors for recycling the unconverted pump radiation. A double-pass fibre amplifier based on fibre Bragg gratings and circulators was demonstrated by Tang et al. [108]. Both schemes, however, require thorough optimisation due to impact of nonlinear effects, sophisticated design, and high sensitivity to environmental perturbations. Amano et al. [109] suggested using a highly nonlinear Raman fibre with a nonlinear coefficient of 6.7 W^{-1} km^{-1} combined with a dispersion compensation fibre (DCF). This highly nonlinear fibre provides an efficient pump conversion while the DCF compensates for the nonlinear distortion added to the signal. Though the modified scheme revealed a more than 50% improvement in terms of pump-to-gain conversion, the noise characteristics degraded due to excessive nonlinear effects.

The promising method for increasing the pump conversion efficiency of the discrete Raman amplifier is based on the combination of the nonlinear Raman fibre with an active fibre in the form of the hybrid amplification scheme. In this scheme it is essential that the spectral gain of an active fibre matches the Raman Stokes band for a single pump source. Using several pump sources would inevitably lead to excessive noise and increase the complexity of the amplifier. When the first stage of a hybrid amplifier, i.e., Raman amplifier, exhibits a low noise figure NF_1 and a relatively high gain G_1, the next amplifier stages made of an active fibre would not notably affect the overall noise figure of the system NF_{sum}, as follows from the analysis of cascaded amplifiers [110]:

$$NF_{sum} = NF_1 + \frac{NF_2 - 1}{G_1} + \frac{NF_3 - 1}{G_1 G_2} + \dots . \qquad (6)$$

Hybrid two-stage (Raman-active fibre) amplifiers operated at the 1.5–1.6-μm spectral range using Er- and Tm-doped fibres and demonstrated superior performance in terms of efficiency and gain bandwidth as compared to single-stage Raman amplifiers [111, 112]. Unfortunately, an efficient active fibre for the 1.3-μm spectral range is still difficult to find. There are expectations that optimised bismuth (Bi) doped fibres would be an appropriate gain medium for the O-band optical communication [52, 98, 113–118]. The gain and pump conversion efficiency demonstrated by the Bi-doped fibres to date are sufficient for several types of optical amplifiers [116, 119]. The broad pump absorbing spectral band allows Bi-doped fibre to share the same pump source with a Raman-amplifier [114, 117, 118].

We have developed a copropagating hybrid fibre Raman-bismuth amplifier based on the experimental setup described in the previous section [98, 120]. The only change in the amplifier scheme shown in Fig. 7 is 60 m of the Bi-doped silica fibre added after 900 m of nonlinear fibre section. The length of the active fibre was chosen to efficiently absorb the residual pump unconverted in the Raman amplifier stage. An active fibre with bismuth ion concentration of 3×10^8 cm^{-3} was manufactured by PCVD technology [117].

Experimental results for the hybrid configuration are demonstrated in Fig. 9. By adding the Bi-doped fibre section an additional 9 dB of the gain has been obtained compared to the single-stage fibre Raman amplifier. For an input signal of 2 mW, the highest gain in hybrid configuration was 18 dB at a pump power of 1.4 W, whereas the fraction of the residual pump was below 3%. The RIN value in the frequency range from 50 MHz to 3 GHz was below –140 dB Hz^{-1}, which is

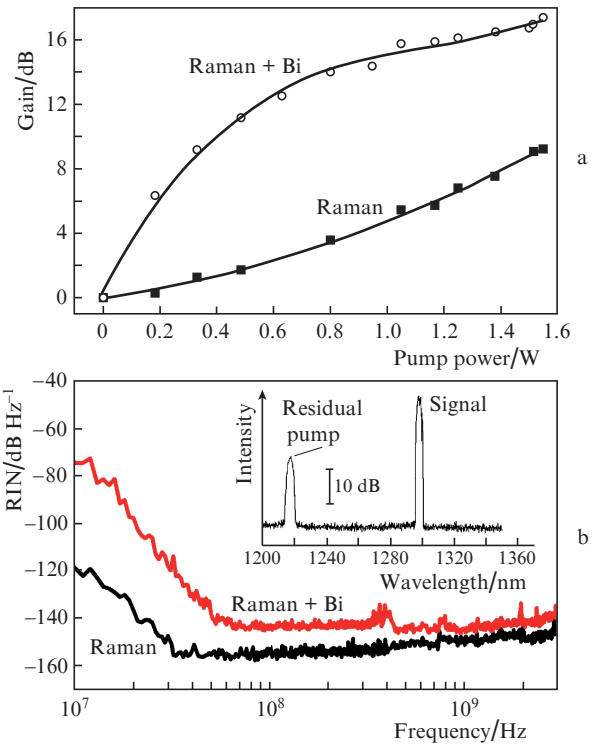

Figure 9. O-band hybrid fibre amplifier performance: (a) small-signal gain vs. pump for a single-stage Raman amplifier and a hybrid two-stage Raman-Bi-doped fibre amplifier, and (b) RIN measurements for a sole fibre Raman amplifier and hybrid configuration. The pump power is 1.1 W. Inset: the output spectrum of the hybrid amplifier.

comparable with single-stage Raman and hybrid amplifiers [15, 103, 111, 116]. The RIN increase in a hybrid amplifier was less than 7 dB (Fig. 9b). The low-frequency RIN increase has the same mechanism as described in the previous section.

The experimental results reported in this section demonstrate the strong potential of SDLs as optical pump sources for both single-stage and hybrid multi-stage Raman fibre amplifiers.

4. Picosecond Raman fibre lasers pumped by an SDL

Fibre Raman lasers are capable of producing ultrashort pulses in the extended spectral range. The vast majority of pulsed Raman lasers reported to date use cw Raman fibre lasers as pump sources (see Table 1). In this section we demonstrate the passively mode-locked Raman fibre lasers pumped by SDLs. Pulsed operation was obtained using nonlinear polarisation rotation (NPR) and semiconductor saturable absorber mirror (SESAM) in both normal and anomalous dispersion regimes [84, 121–123].

4.1. Picosecond fibre Raman laser mode-locked with a semiconductor saturable absorber mirror

We used a 1.48-μm SDL as a pump source of a mode-locked Raman fibre laser operating at 1.59 μm [122]. The active medium of the SDL was grown by MBE on the InP substrate. The gain medium comprised 8 compressively strained AlGaInAs quantum wells. The distributed Bragg reflector grown by solid-source MBE consisted of 35 pairs of quarter-wave thick $Al_{0.9}Ga_{0.1}As$ and GaAs layers. The reflector and the gain medium were processed using a 2-inch wafer fusion technique [124]. After the fusion step, the InP-substrate and GaInAsP etch-stop layer were selectively etched by wet etching and cut into 2.5 × 2.5-mm chips. The active mirror was placed on a water-cooled copper holder. A 200-μm-thick diamond heat spreader was then bonded on the top surface of the sample. The InP cap layer and the surface of the diamond are pulled together by intermolecular forces of water. The cavity of the disk laser was of V-type (Fig. 5) and composed of a 97.5%-reflective plane output coupler, spherical mirror and gain mirror. The gain mirror was pumped with a 980-nm fibre-coupled diode laser. The pump is focused to the gain mirror to a spot of 180 μm in diameter. The cavity was designed to ensure that the mode size at the gain mirror matches the pump spot. The output beam quality parameter was less than 1.5. The maximum output power launched in the single mode fibre was 1.7 W, corresponding to the coupling efficiency of 75%.

The laser cavity setup is demonstrated in Fig. 10. A semiconductor saturable absorber mirror (SESAM) was inserted into the cavity to ensure the start-up of mode-locking [125]. The both cavity mirrors were butt-coupled with an optical fibre. It is important to note that the SESAM nonlinear parameters can be optimised for a wide spectral range of the pulse wavelengths and durations from several femtoseconds to tens of nanoseconds. SEASAMs can be tailored for solid-state, semiconductor, and fibre laser systems [126].

A 450-m-long highly GeO_2-codoped silica fibre acted as a Raman gain medium. The fibre had an effective mode area at 1.55 μm, 10.4 μm^2; core/cladding refractive index difference, Δn = 0.03; and passive loss at the signal wavelength,

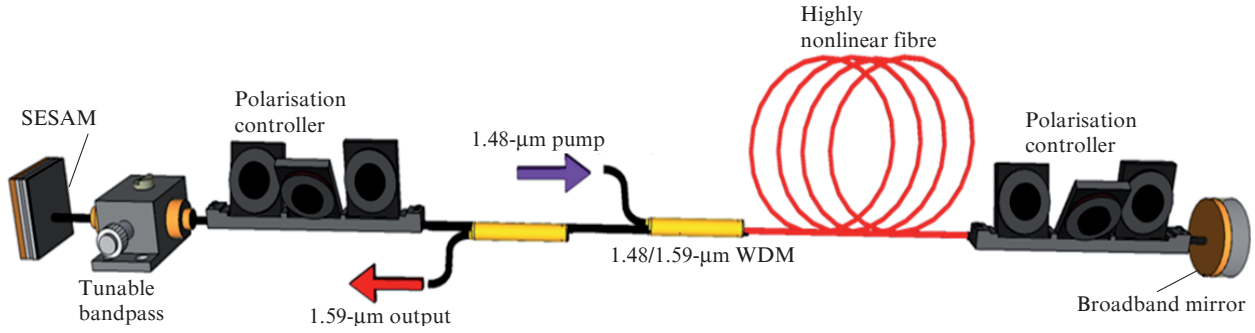

Figure 10. Schematic of a linear-cavity passively mode-locked Raman fibre laser.

1.5 dB km^{-1}. The fibre dispersion of 19.46 ps nm^{-1} km^{-1} resulted in a total cavity dispersion of 2.5 ps nm^{-1}.

The polarisation controllers were employed to stabilise the laser operation due to sufficiently high intracavity powers and high nonlinearity. A tunable optical filter was used to control the parameters of the generated pulses [40]. The signal was coupled out through a 1% fibre coupler.

The output optical spectrum of the pulsed laser is shown in Fig. 11a. It should be noted that the start-up of mode-locking in Raman fibre lasers differs significantly from the pulse development in rare-earth doped fibre lasers. Because the gain relaxation dynamics in rare-earth doped glasses is slow (from 100 μs to 10 ms) [110], it enables the efficient energy storage in the laser cavity which usually provokes the evolution to steady-state mode-locking through the Q-switching instability. On the other hand, the Raman gain exhibits fast gain dynamics with femtosecond relaxation times τ_R [30], which are shorter than cavity round-trip time τ_{pass}.

This condition prevents energy storage in the cavity, which is a prerequisite for the Q-switching instability development and, as a result, there develops a mode-locked pulse train from spontaneous noise radiation (see oscillograms in Fig. 11b). This qualitative description explains an increase in the length of the pulse train envelope with pump power. Eventually, at a sufficient pump power, the transition to actual cw mode-locking occurs, when all the time slots are filled and uniform pulse pattern builds up without a low-frequency envelope.

The tunable bandpass spectral filter with a 1–10-nm bandwidth was used in the cavity to optimise mode-locked operation of the fibre Raman laser [38, 40, 127]. The pump power threshold for a mode-locked operation was ~400 mW, and the shortest pulse was observed at a pump power of 1 W. The pulse characteristics of the mode-locked train with the repetition rate of 170 kHz are shown in Fig. 12. The pulse duration derived from the autocorrelation trace was 2.7 ps, corresponding to the time-bandwidth product of 0.68, which indicates the high quality of the pulsed regime. Some noise around the pulse on the autocorrelation trace (Fig. 12a) is likely due to a low modulation depth of the SESAM which

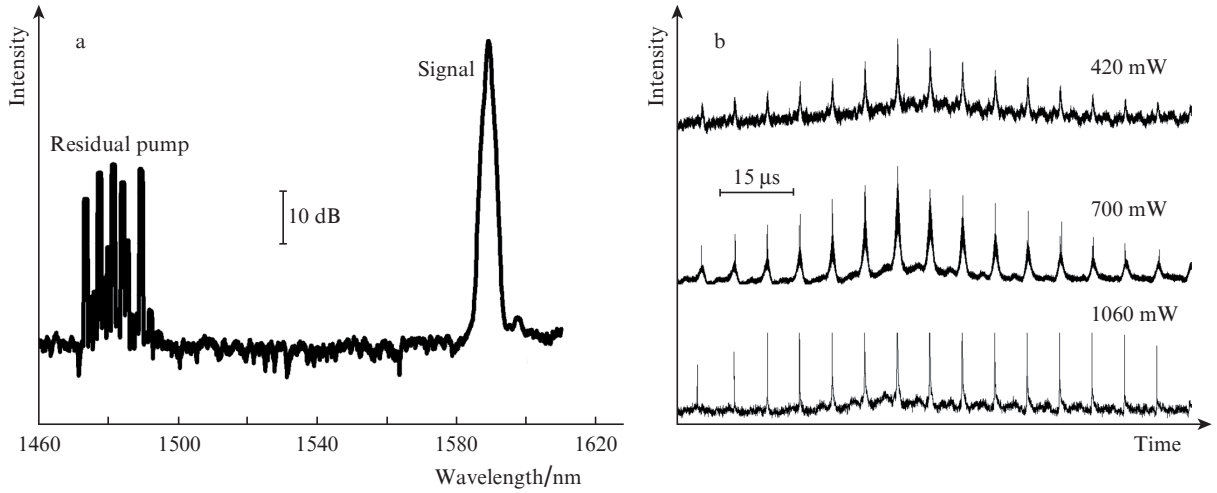

Figure 11. (a) Output optical spectrum of a Raman laser, radiation in the region of 1480 nm is caused by residual pump, and (b) oscilloscope traces of the output pulsed signal from a passively mode-locked Raman fibre laser at different pump powers.

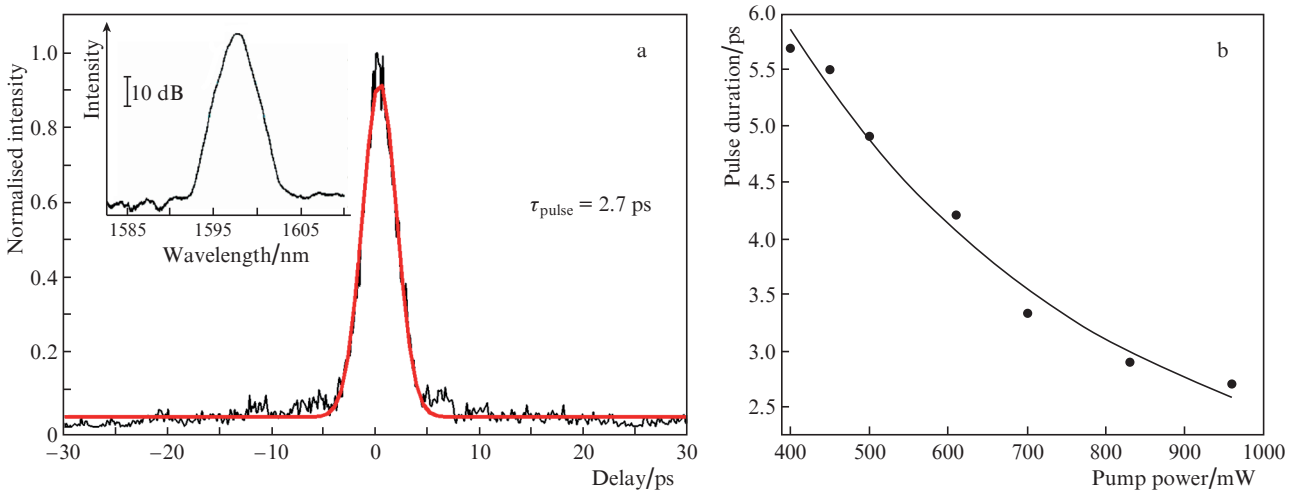

Figure 12. (a) Autocorrelation trace with sech^2-fitting and optical spectrum of the mode-locked Raman laser with a SESAM, and (b) pulse duration vs. pump power.

was below 10%. The pulse duration decreases with increasing pump power (Fig. 12b). With 1% output coupler, the maximum average power was 60 mW. Once the mode-locking sets in (Fig. 10), the laser operation remained stable.

Thus, a 1.59-μm passively mode-locked Raman fibre laser pumped by a 1480-nm wafer-fused semiconductor disk laser was demonstrated. SESAM mode-locking combined with highly nonlinear fibre allows a relatively short cavity 450 m long to be built and results in a stable pulse operation. The efficient pump scheme offered by the SDL combined with SESAM technology has a promising potential for application in pulsed Raman oscillators.

4.2. Picosecond Raman fibre laser with nonlinear polarisation rotation

The saturable absorption mechanism based on nonlinear polarisation rotation (NPR) is wavelength independent and allows one to preserve all-fibre configuration of the mode-locked Raman fibre laser. Below the NPR technique together with optical pumping by the 1.3-μm SDL is applied to the ring cavity Raman fibre laser [84].

The experimental setup of the picoseconds fibre laser is shown in Fig. 13. The 1.3-μm SDL pump source comprises a semiconductor gain mirror with 10 AlGaInAs quantum wells and a distributed Bragg reflector with 35 $Al_{0.9}Ga_{0.1}As/GaAs$ layers. The polarisation isolator served as a discriminator of the pulsed regime. The mode-locking was performed by tuning the polarisation controllers. The output beam quality parameter was better than $M^2 < 1.4$ and allowed radiation (more than 2 W) to be launched into the single-mode fibre with the efficiency ~70%. A 650-m-long nonlinear silica fibre used as a Raman gain medium was similar to the one described in the previous section. The lasing was observed at the first Stokes band at 1.38 μm by pumping at 1.3 μm (Fig. 14a). Unlike the previous experiment, the laser operated in the normal dispersion regime with the total cavity dispersion at the signal wavelength of –7.41 ps nm^{-1}. Since the pulse energy is not limited by soliton shaping in this regime and, consequently, the multiple pulsing is avoided, the high energy pulses can be produced without pulse breaking [128–130]. The threshold of mode-locking regime was ~300 mW and the highest value of average output power of 70 mW was achieved at 1 W of pump power (Fig. 14b). The shortest pulse duration estimated from a $sech^2$-fitting of autocorrelation trace was 1.97 ps (Fig. 14c). Owing to relatively short-length cavity and, consequently, low value of cavity dispersion, the time-bandwidth product of the pulses was 0.69, which is only 1.36 times higher than the transform-limited value. Thus, the application of stable and low-noise pump SDLs makes it possible to produce fibre Raman lasers emitting short pulses at different wavelengths (including 1.38-μm pulses), which are unavailable for the gain media based on rare-earth-doped fibres.

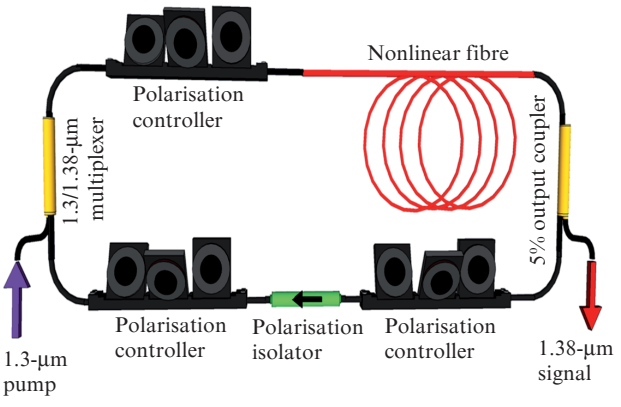

Figure 13. Schematic of a picosecond Raman fibre laser mode-locked with nonlinear polarisation rotation.

5. Supercontinuum generation using semiconductor disk lasers

In addition to applications in fibre Raman oscillators, SDLs can be employed in other types of the nonlinear-optic devices. Ultrabroadband signal generation, also known as supercontinuum generation, is regularly obtained with high power ultrashort solid-state or fibre lasers [131]. As a matter of fact, the requirements imposed on the pump sources for Raman and supercontinuum devices are similar in many respects: the efficient light coupling of high power into a small-core single-mode fibre is a primary objective for both supercontinuum generators and Raman devices. Mode-locked SDLs can be an interesting alternative to modern pump sources of supercontinuum generators. Pulsed SDLs have a number of significant advantages: stable picosecond pulse generation, diffraction-limited output beam and the opportunity for mode-locked operation at the extended spectral range from 900 nm to 1600 nm [61, 132–134]. Therefore, the SDL is a promising candidate for supercontinuum generation. Below we demonstrate supercontinuum generation in a nonlinear optical fibre using the picosecond 1.57-μm SDL. This scheme could of interest for broadband WDM communication and high resolution optical sensing and detection [135].

The fabrication of high-power SDLs operating in the 1.5-μm spectral band requires a number of issues to be addressed. The active gain medium of such lasers relies on InP structures, which are the main material for this spectral range. Until recently, such sources were fabricated by growing the active medium and a distributed mirror, necessary for the implementation of the vertical geometry of the structure during a single-step epitaxial process. However, the monolithic growth process of InP-based gain mirrors used to date suffers from the low refractive index contrast of the layers forming the distributed Bragg reflector [1]. Consequently, the large number of layers (50 or more) required for growth of a high-reflectivity reflector induces a significant penalty to thermal properties of the gain element. Continuous-wave output power from 1.5-μm SDLs using monolithic structure, grown by a single-step epitaxial process, was limited to 160 mW at room temperature and to 800 mW at –33°C [136, 137]. 120-mW, 3.2-ps pulses were obtained in the mode-locked regime at –22°C [138]. Another methods based on metamorphic growth or using dielectric distributed reflectors allowed the power up to 80 mW to be obtained in the cw regime [139, 140]. This power, however, is well below the level required for supercontinuum applications.

The wafer fusion technology, which allows one to combine the advantages of InP and GaAs semiconductors, which can be grown monolithically without many defects, was shown to be a promising technique for fabrication of long-wavelength high-power SDLs [78]. Using this technology, a 1.57-μm SDL with a GaAs/AlGaAs-based distributed Bragg reflector and InP-based active medium producing 4.6 W of output power at room temperature was developed [85]. In the

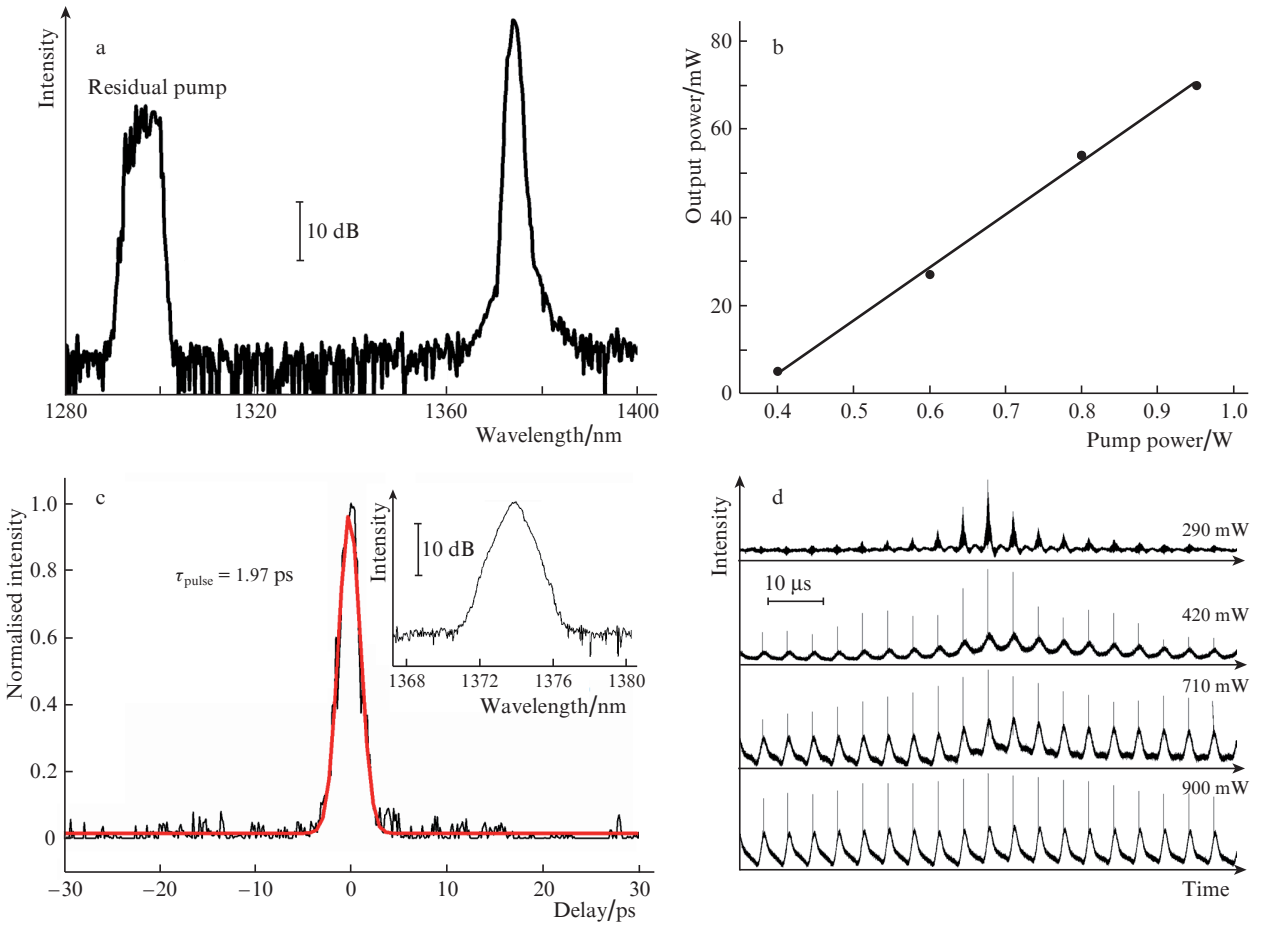

Figure 14. Output characteristics of a fibre Raman laser passively mode-locked with nonlinear polarisation rotation: (a) output optical spectrum, (b) signal output vs. pump power, (c) autocorrelation trace with $sech^2$-fitting (inset: the corresponding optical spectrum), and (d) oscilloscope traces of the pulse train evolution vs. pump power.

mode-locked regime, the laser generated 16-ps pulses with 0.86 W of average output power [141]. This power level of pulsed SDLs is suitable for pumping supercontinuum generators.

Using the wafer-fusion technique, the SDL generating 14.4-ps pulses with a repetition rate of 1.6 GHz, average power of 400 mW and the central wavelength of 1.565 μm has been developed. The pulsed output of the SDL was further launched into an Yb/Er-doped fibre amplifier to boost an output power. The amplified signal with an average power of 4.5 W then coupled into a 500-m-long nonlinear highly GeO_2-codoped silica fibre produced spectral continuum spanning from 1.35 μm to 2 μm. This is the first demonstration of supercontinuum generation using the pulsed 1.5-μm SDL-based system. Another successful demonstration of this concept reported recently for a 1-μm SDL amplified with an Yb-doped multi-stage fibre amplifier reports 4-ps output pulses with an average power above 200 W [142].

5.1. High power picosecond hybrid 1.57 μm semiconductor disk laser

The schematic of the pulsed SDL is shown in Fig. 15a. The active semiconductor mirror includes a gain section comprised of 10 layers of AlGaInAs/InP quantum wells grown on a GaAs substrate. The active section was wafer fused with the distributed Bragg reflector made of 35 $Al_{0.9}Ga_{0.1}As$/GaAs

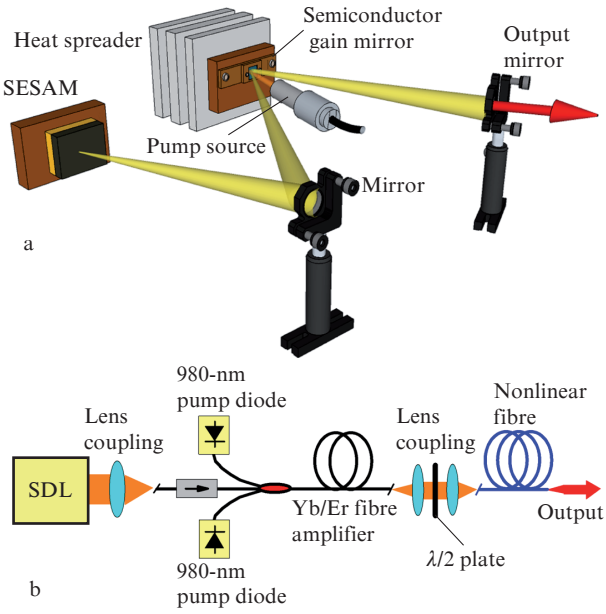

Figure 15. (a) Schematic of a passively mode-locked SDL cavity, and (b) experimental setup of supercontinuum generation with a passively mode-locked SDL (fibre ends are angle cleaved to prevent the spurious reflections and a waveplate is introduced to control supercontinuum generation performance).

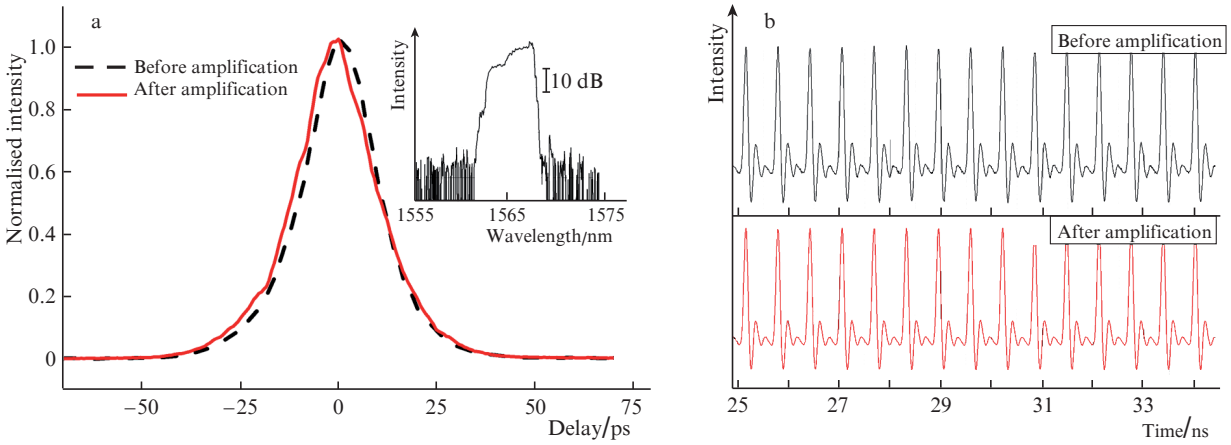

Figure 16. (a) Output pulse autocorrelation trace with sech2-fitting before and after the amplification (inset: optical spectrum of the amplified pulse), and (b) oscilloscope traces of the original and amplified pulse trains.

layers. Both structures were grown using solid-source MBE [141]. Wedged intracavity diamond heat spreader was bonded onto the gain element to ensure an efficient heat removal. The temperature of the laser was kept at 15–17°C by means of water cooling. A 980-nm fibre-coupled multimode laser diode was used as a pump source for an SDL.

Mode-locking was achieved with a GaInNAs-based SESAM [61, 143]. With 14.1 W of pump power the laser produced 400 mW of average output power. Figure 16a demonstrates the autocorrelation trace and optical spectrum of the output pulse train. The 14.4-ps pulse duration was derived from the autocorrelation trace by $sech^2$-fitting. The measured pulse repetition rate of 1.6 GHz is twice the fundamental repetition rate of the SDL cavity (Fig. 16b). The stable operation at higher harmonics is frequently observed in SDLs due to the fast recovery time of the gain medium and dynamic gain saturation [144].

The laser output was focused into an angle cleaved single-mode fibre, followed by an optical isolator to avoid feedback to the SDL and to ensure unidirectional amplification (Fig. 15b). 100 mW of average power was measured after the optical isolator. The SDL output pulses were amplified in a 5.5-m-long Er/Yb-doped fibre (Nufern SM-EYDF-7/130) amplifier pumped by two 980-nm diodes. The highest average output power obtained after amplification was 4.5 W, corresponding to pulse energy of 2.8 nJ. The amplified pulse duration was 15.5 ps (Fig. 16a). The amplified signal was then coupled into a nonlinear fibre. The nonlinear silica fibre had the GeO_2 concentration of 30 mol % and the length of 500 m. The core/cladding index difference, numerical aperture and zero dispersion wavelength of the fibre were $\Delta n = 0.03$, 0.25 and 1530 nm, respectively. The cut-off wavelength and the calculated nonlinear coefficient of the fibre were 1390 nm and $\gamma = 8.4\ W^{-1}\ km^{-1}$. The zero dispersion wavelength of the nonlinear fibre was chosen to be close to the SDL operation wavelength to facilitate better conversion to ultrabroad spectrum [131].

5.2. Supercontinuum generation using short pulse semiconductor disk laser

Supercontinuum spectra for different pump powers are shown in Fig. 17. The optical spectrum ranging from 1320 nm to 2000 nm (measured at a 20-dB level) with an output power

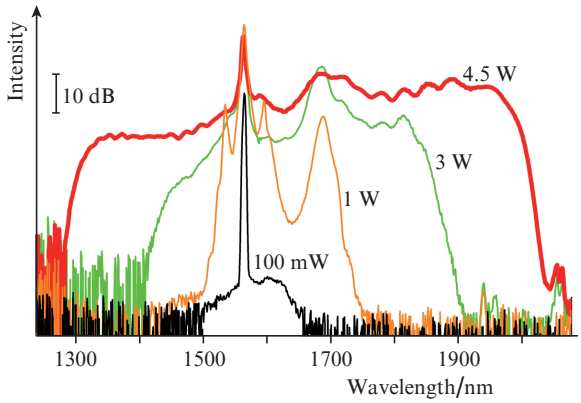

Figure 17. Optical spectra at the output of a 500-m-long nonlinear fibre, measured at different pump power levels.

of 3.5 W was obtained for a launched pump power of 4.5 W. The width and the spectral shape of the supercontinuum could be adjusted with the help of polarisation of the input signal.

Thus, the supercontinuum generation using a 1.57-μm passively mode-locked semiconductor disk laser was demonstrated. To our knowledge this is the first demonstration of supercontinuum generation using SDL pumping [145].

6. Conclusions

The semiconductor disk lasers technology has been demonstrated to be an effective means for optical pumping of fibre Raman lasers and amplifiers. This relatively novel type of lasers could operate with a low relative intensity noise (–150 dB Hz^{-1}) combined with a scalable multiwatt output power and nearly diffraction-limited beam quality, which allows an efficient light coupling into single mode fibre. To date, semiconductor disk lasers are capable of operating in a spectral range from 250 nm to 2.5 μm.

Using semiconductor disk lasers, low-noise fibre Raman amplifiers in the copropagation configuration were developed for the 1.3-μm spectral range. A hybrid Raman-bismuth-doped fibre amplifier was proposed for an efficient pump light conversion with the gain up to 18 dB. The possibility of fabricating picosecond Raman mode-locked fibre lasers oper-

ating in both normal and anomalous dispersion regimes was demonstrated experimentally. Semiconductor disk lasers operating at 1.29 μm and 1.48 μm were used as the pump sources for short pulse Raman oscillators. The 1.38-μm passively mode-locked all-fibre Raman fibre laser produced 1.97-ps pulses with an average output power of 70 mW in the normal dispersion regime. The 1.59-μm fibre laser with the integrated semiconductor saturable absorber mirror generated 2.7-ps pulses with an average power of ~60 mW. By utilising a picosecond semiconductor disk laser amplified in ytterbium-erbium doped fibre amplifier, the supercontinuum generation spanning from 1.35 μm to 2 μm with an average power of 3.5 W was achieved.

The experimental results show promising opportunities offered by the semiconductor disk laser technology for application in the nonlinear optics.

Acknowledgements. The authors express their gratitude to K.M. Golant and Yu.K. Chamorovskiy (Kotel'nikov Institute of Radioengineering and Electronics, Russian Academy of Sciences) for providing nonlinear and active bismuth-doped fibre samples. The authors would like to thank A. Sirbu, A. Mereuta, A. Caliman and E. Kapon from École Polytechnique Fédérale de Lausanne, Switzerland for their help with wafer-fused disk laser technology. The experimental study was assisted by A. Rantamäki, J. Rautiainen, E.J. Saarinen, J. Kerttula, J. Lyytikäinen, T. Leinonen and J. Puustinen from the Optoelectronics Research Centre, Tampere University of Technology, Finland.

References

1. Okhotnikov O.G. *Semiconductor Disk Lasers: Physics and Technology* (Weinheim: Wiley-VCH, 2010).
2. Landsberg G., Mandelstam L. *Z. für Physik*, **50**, 769 (1928).
3. Raman C.V., Krishnan K.S. *Nature*, **121**, 501 (1928).
4. Geller M., Bortfeld D.P,. Sooy W.R, Woodbury E.J. *Proc. IEEE*, **51**, 1236 (1963).
5. Stolen R.H., Ippen E.P. *Appl. Phys. Lett*., **22**, 276 (1973).
6. Bromage J. *J. Lightwave Technol*., **22**, 79 (2004).
7. Mollenauer L.F., Stolen R.H. *Opt. Lett*., **9**, 13 (1984).
8. Mollenauer L., Gordon J., Islam M. *IEEE J. Quantum Electron*., **22**, 157 (1986).
9. Grubb S., Erdogan T., Mizrahi V., Strasser T., Cheung W., Reed W., Lemaire P., Miller A., Kosinski S., Nykolak G. *Opt. Ampl.Appl.*, **14**, PD3 (1994).
10. Dianov E.M., Grekov M.V., Bufetov I.A., Vasiliev S.A., Medvedkov O.I., Plotnichenko V.G., Koltashev V.V., Belov A.V., Bubnov M.M., Semjonov S.L. *Electron. Lett*., **33**, 1542 (1997).
11. Masuda H., Aida K. *Opt. Ampl. Appl.*, **18**, ThE2 (1995).
12. Andre P.S., Pinto A.N., Teixeira A.L.J., Neto B., Junior S., Spertti D., da Rocha F., Bernardo M., Fujiwara M., Rocha A., Facao M. *Transparent Optical Networks ICTON '07*, **1**, 136 (2007).
13. Headley C., Agrawal G.P. *Raman Amplification in Fiber Optical Communication Systems* (New York: Acad. Press, 2005).
14. Mohamed A.E.N.A., Rashed A.N.Z., Eid M.M.A. *Intern. J. Computer Sci. Technol.*, **3**, 784 (2012).
15. Islam M.N. *IEEE J. Select. Top. Quantum Electron*., **8**, 548 (2002).
16. Dianov E.M., Prokhorov A.M. *IEEE J. Select. Top. Quantum Electron*., **6**, 1022 (2000).
17. Meltz G., Morey W.W., Glenn W.H. *Opt. Lett*., **14**, 823 (1989).
18. Kravtsov K.S., Bufetov I.A., Medvedkov O.I., Dianov E.M., Yashkov M.V., Gur'yanov A.N. *Kvantovaya Elektron*., **35**, 586 (2005) [*Quantum Electron*., **35**, 586 (2005)].
19. Feng Y., Taylor L.R., Calia D.B. *Opt. Express*, **17**, 23678 (2009).
20. Feng Y., Huang S., Shirakawa A., Ueda K.-I. *Jpn. J. Appl. Phys*., **43**, L722 (2004).
21. Feng Y., Taylor L.R., Calia D.B. *Opt. Express*, **17**, 19021 (2009).
22. Xiong Z., Moore N., Li Z.G., Lim G.C. *J. Lightwave Technol.*, **21**, 2377 (2003).
23. Codemard C.A., Ji J., Sahu J.K., Nilsson J. *Laser*, **80**, 120 (2010).
24. Codemard C.A., Sahu J.K., Nilsson J. *Tech. Dig. OFC/FOEC* (Anaheim, USA, 2005) Vol. 2, paper OTuF5.
25. Codemard C.A., Nilsson J., Sahu J. *Tech. Digest CLEO/QELS 2007* (Baltimore, USA, 2007) paper CTuN3.
26. Fludger C., Handerek V., Mears R. *J. Lightwave Technol*., **19**, 1140 (2001).
27. Bouteiller J. *Ann. Telecommun.*, **58**, 1342 (2003).
28. Dianov E.M., Bufetov I.A., Mashinsky V.M., Shubin A.V., Medvedkov O.I., Rakitin A.E., Mel'kumov M.A., Khopin V.F., Gur'yanov A.N. *Kvantovaya Elektron*., **35**, 435 (2005) [*Quantum Electron*., **35**, 435 (2005)].
29. Agrawal G.P. *Fiber-Optic Communication Systems* (New York: Wiley, 1997) Vol. 3.
30. Stolen R.H., Gordon J.P., Tomlinson W.J., Haus H.A. *J. Opt. Soc. Am. B*, **6**, 1159 (1989).
31. Ohki Y., Hayamizu N., Shimizu H., Irino S., Yoshida J., Tsukiji N., Namiki S. *OSA Trends Opt. Photon. Series*, **77**, PD7 (2002).
32. Namiki S., Seo Koji, Tsukiji N., Shikii S. *Proc. IEEE*, **94**, 1024 (2006).
33. Yoshida J., Tsukiji N., Kimura T., Funabashi M., Fukushima T. *Proc. SPIE Int. Soc. Opt. Eng*., **4870**, 169 (2002).
34. Bolognini G., Sugliani S., Di Pasquale F. *IUST Photonics* (Cochin, India, 2004) paper FBR 1.1.
35. Kbashi H.J., Al-Naimee K., Jawad H., Benocci R., Narayanan V., Batani D. *Appl. Phys. Res*., **2**, 55 (2010).
36. Schröder J., Alasia D., Sylvestre T., Coen S. *J. Opt. Soc. Am. B*, **25**, 1178 (2008).
37. Schröder J., Coen S., Vanholsbeeck F., Sylvestre T. *Opt. Lett*., **31**, 3489 (2006).
38. Chestnut D.A., Taylor J.R. *Opt. Lett*., **30**, 2982 (2005).
39. Aguergaray C., Mochin D., Kruglov V., Harvey J.D. *Opt. Express*, **18**, 8680 (2010).
40. Castellani C.E.S., Kelleher E.J.R., Travers J.C., Popa D., Hasan T., Sun Z., Flahaut E., Ferrari A.C., Popov S.V., Taylor J.R. *Opt. Lett*., **36**, 3996 (2011).
41. Castellani C.E.S., Kelleher E.J.R., Luo Z., Wu K., Ouyang C., Shum P.P., Shen Z., Popov S.V., Taylor J.R. *Laser Phys. Lett*., **9**, 223 (2012).
42. Bonaccorso F., Sun Z., Hasan T., Ferrari A. C. *Nat. Photon.*, **4**, 611 (2010).
43. Sun Z., Hasan T., Ferrari A.C. *Physica E*, **44**, 1082 (2012).
44. http://www.oclaro.com/brochures/OCL_BR_HPLD_2012-01_NonPrint.pdf.
45. Namiki S., Tsukiji N., Emori Y., in *Raman Amplifiers for Telecommunications 1*, Islam M. (Ed.) (Berlin: Springer, 2004) Vol. 90, p. 121.
46. Tsukiji N., Hayamizu N., Shimizu, Y. Ohki H., Kimura T., Irino S., Yoshida J., Fukushima T., Namiki S. *Opt. Ampl. Appl.*, **77**, PD7 (2002).
47. Ohki Y., Hayamizu N., Irino S., Shimizu H., Yoshida J., Tsukiji N. *Furukawa Rev.*, **24**, 6 (2003).
48. Dianov E.M. *J. Lightwave Technol*., **20**, 1457 (2002).
49. http://www.ipgphotonics.com.
50. Moulton P.F., Rines G.A., Slobodtchikov E.V., Wall K.F., Frith G., Samson B., Carter A.L.G. *IEEE J. Sel.Top. Quantum Electron*., **15**, 85 (2009).
51. Sahu J.K., Jeong Y., Richardson D.J., Nilsson J., in *Advanced Sol. State Photon. 2005* (Vienna, 2005) p. MB33.
52. Dianov E.M., Shubin A.V., Melkumov M.A., Medvedkov O.I., Bufetov I.A. *J. Opt. Soc. Am. B,* **24**, 1749 (2007).
53. Yi L., Zhan L., Hu W., Hu P., Su Y., Leng L., Xia Y. *IEEE Photon. Technol. Lett*., **18**, 1028 (2006).
54. Strutz S.J., Williams K.J. *Electron. Lett*., **36**, 1359 (2000).
55. Geng J., Staines S., Wang Z., Zong J., Blake M., Jiang S. *IEEE Photon. Technol. Lett*., **18**, 1813 (2006).
56. Bufetov I.A., Bubnov M.M., Larionov Y.V., Medvedkov O.I., Vasiliev S.A., Melkoumov M.A., Rybaltovsky A.A., Semjonov S.L., Dianov E.M., Gur'yanov A.N. *Laser Phys.*, **13**, 234 (2003).
57. Zhao Y., Jackson S. *Opt. Express*, **13**, 4731 (2005).

58. Rini M., Cristiani I., Degiorgio V. *IEEE J. Quantum Electron.*, **36**, 1117 (2000).
59. Kitayama Y., Tanaka S. *Electron. Commun. Jpn (P. I: Commun.)*, **68**, 104 (1985).
60. Kalyoncu S.K., Gao S., Tien E.-K., Huang Y., Yildirim D., Adas E., Wabnitz S., Boyraz O. *J. Opt. Soc. Am. B*, **28**, 2812 (2011).
61. Okhotnikov O.G. *Kvantovaya Elektron*., **38**, 1083 (2008) [*Quantum Electron*., **38**, 1083 (2008)].
62. Giesen A., Speiser J. *IEEE J. Select. Top. Quantum Electron*., **13**, 598 (2007).
63. Tropper A.C., Foreman H.D., Garnache A., Wilcox K.G., Hoogland S.H. *J. Phys. D: Appl. Phys*., **37**, R75 (2004).
64. Vul B.M., Keldysh L.V., Kotel'nikov V.A., Logunov A.A., Markov M.A., Nikol'skii S.I., Plotnikov A.F., Prokhorov A.M., Skobel'tsyn D.V. *Usp. Fiz. Nauk*, **138** (4), 683 (1982) [*Sov. Phys. Usp*., **25**, 940 (1982)].
65. Basov N.G. *Nobel Lectures Physics*, **1963–1970**, 89 (1998).
66. Jiang W.B., Friberg S.R., Iwamura H., Yamamoto Y. *Appl. Phys. Lett*., **58**, 807 (1991).
67. Jiang W.B., Mirin R., Bowers J.E. *Appl. Phys. Lett*., **60**, 677 (1992).
68. Kuznetsov M., Hakimi F., Sprague R., Mooradian A. *IEEE Photon. Technol. Lett*., **9**, 1063 (1997).
69. Morton L.G., Hastie J.E., Dawson M.D., Krysa A.B., Roberts J.S. *CLEO/QELS 2006* (Long Beach, USA, 2006) p. JWB16.
70. Hastie J., Calvez S., Dawson M., Leinonen T., Laakso A., Lyytikäinen J., Pessa M. *Opt. Express*, **13**, 77 (2005).
71. Beyertt S.-S., Brauch U., Demaria F., Dhidah N., Giesen A., Kubler T., Lorch S., Rinaldi F., Unger P. *IEEE J. Quantum Electron*., **43**, 869 (2007).
72. Chilla J., Butterworth S., Zeitschel A., Charles J., Caprara A., Reed M., Spinelli L. *Proc. SPIE Int. Soc. Opt. Eng*., **5332**, 143 (2004).
73. Rudin B., Rutz A., Hoffmann M., Maas D.J.H.C., Bellancourt A.-R., Gini E., Südmeyer T., Keller U. *Opt. Lett*., **33**, 2719 (2008).
74. Lutgen S., Albrecht T., Brick P., Reill W., Luft J., Späth W. *Appl. Phys. Lett*., **82**, 3620 (2003).
75. Korpijärvi V.-M., Guina M., Puustinen J., Tuomisto P., Rautiainen J., Härkönen A., Tukiainen A., Okhotnikov O., Pessa M. *J. Crystal Growth*, **311**, 1868 (2009).
76. Korpijärvi V.-M., Leinonen T., Puustinen J., Härkönen A., Guina M.D. *Opt. Express*, **18**, 25633 (2010).
77. Lyytikäinen J., Rautiainen J., Toikkanen L., Sirbu A., Mereuta A., Caliman A., Kapon E., Okhotnikov O.G. *Opt. Express*, **17**, 9047 (2009).
78. Rautiainen J., Lyytikäinen J., Sirbu A., Mereuta A., Caliman A., Kapon E., Okhotnikov O.G. *Opt. Express*, **16**, 21881 (2008).
79. Lyytikäinen J., Rautiainen J., Sirbu A., Iakovlev V., Laakso A., Ranta S., Tavast M., Kapon E., Okhotnikov O.G. *IEEE Photon. Technol. Lett*., **23**, 917 (2011).
80. Hopkins J.-M., Hempler N., Rösener B., Schulz N., Rattunde M., Manz C., Köhler K., Wagner J., Burns D. *Opt. Lett*., **33**, 201 (2008).
81. Schulz N., Rattunde M., Ritzenthaler C., Rosener B., Manz C., Kohler K., Wagner J., Brauch U. *Appl. Phys. Lett*., **91**, 091113 (2007).
82. Rautiainen J., Härkönen A., Korpijärvi V.-M., Tuomisto P., Guina M., Okhotnikov O.G. *Opt. Express*, **15**, 18345 (2007).
83. McInerney J.G. *Proc. SPIE Int. Soc. Opt. Eng*., **4994**, 21 (2003).
84. Chamorovskiy A., Rantamäki A., Sirbu A., Mereuta A., Kapon E., Okhotnikov O.G. *Opt. Express*, **18**, 23872 (2010).
85. Rantamäki A., Rautiainen J., Lyytikäinen J., Sirbu A., Mereuta A., Kapon E., Okhotnikov O.G. *Opt. Express*, **20**, 9046 (2012).
86. Rantamäki A., Sirbu A., Mereuta A., Kapon E., Okhotnikov O. G. *Opt. Express*, **18**, 21645 (2010).
87. Kardosh I., Demaria F., Rinaldi F., Riedl M.C., Michalzik R. *Electron. Lett*., **44**, 524 (2008).
88. Mooradian A. *Opt. Fiber Commun. Conf. 2001* (Anaheim, USA, 2001) Vol. 4, p. PD17.
89. Bousseksou A., Kurdi M.E., Salik M.D., Sagnes I. *Bouchoule S. Electron. Lett*., **40**, 1490 (2004).
90. Kurdi M.E., Bouchoule S., Bousseksou A., Sagnes I., Plais A., Strassner M., Symonds C., Garnache A., Jacquet J. *Electron. Lett*., **40**, 671 (2004).
91. Keller U., Tropper A.C. *Phys. Reports*, **429**, 67 (2006).
92. Baili G., Bretenaker F., Alouini M., Morvan L., Dolfi D., Sagnes I. *J. Lightwave Technol*., **26**, 952 (2008).
93. Pal V., Trofimoff P., Miranda B.-X., Baili G., Alouini M., Morvan L., Dolfi D., Goldfarb F., Sagnes I., Ghosh R., Bretenaker F. *Opt. Express*, **18**, 5008 (2010).
94. Silfvast W.T. *Laser Fundamentals* (Cambridge: Cambridge Univ. Press, 2004).
95. Senior J. M., Jamro M. Y. *Optical Fiber Communications: Principles and Practice* (Harlow: Pearson Education, 2008).
96. Nishida Y., Yamada M., Kanamori T., Kobayashi K., Temmyo J., Sudo S., Ohishi Y. *IEEE J. Quantum Electron*., **34**, 1332 (1998).
97. Ohishi Y., Kanamori T., Kitagawa T., Takahashi S., Snitzer E., Sigel J. *Opt. Lett*., **16**, 1747 (1991).
98. Chamorovskiy A., Rautiainen J., Rantamäki A., Golant K.M., Okhotnikov O.G. *Opt Express*, **19**, 6433 (2011).
99. Chamorovskiy A., Rautiainen J., Rantamäki A., Okhotnikov O.G. *Opt. Express*, **19**, 6414 (2011).
100. Rautiainen J., Toikkanen L., Lyytikäinen J., Sirbu A., Mereuta A., et al. *CLEO Conf. Dig.* (Munich, 2009) p. CB5_3.
101. Sirbu A., Volet N., Mereuta A., Lyytikäinen J., Rautiainen J., Okhotnikov O., Walczak J., Wasiak M., Czyszanowski T., Caliman A., Zhu Q., Iakovlev V., Kapon E. *Adv. Opt.Technol*., **2011**, 1 (2011).
102. Hui R., O'Sullivan M. *Fiber Optic Measurement Techniques* (New York: Acad. Press, 2009).
103. Ahmad A., Md Ali M.I., Zamzuri A.K., Mohamad R., Mahdi M.A. *Microwave Opt. Technol. Lett*., **48**, 721 (2006).
104. Aoki Y. *J. Lightwave Technol*., **6**, 1225 (1988).
105. Ball G.A., Hull-Allen G., Holton C., Morey W.W. *Electron. Lett*., **29**, 1623 (1993).
106. Sun G., Cai Z., Ye C. *Opt. Commun*., **260**, 645 (2006).
107. Nicholson J.W. *J. Lightwave Technol*., **21**, 1758 (2003).
108. Tang M., Gong Y.D., Shum P. *J. Lightwave Technol*., **22**, 1899 (2004).
109. Amano T., Okamoto K., Tsuzaki T., Kakui M., Shigematsu M. *OFC 2003* (Atlanta, 2003) p. WB3.
110. Desurvire E. *Erbium Doped Fiber Amplifiers* (New York: John Wiley & Sons Inc., 1994).
111. Masuda H. *Techn. Dig. Opt. Fiber Commun. Conf.* (OSA, 2000) Vol. 1, p. TuA1.
112. Lee J., Chang Y.,. Han Y.-G, Kim S. H., Chung H., Lee S.B. *IEEE Photon. Technol. Lett*., **17**, 43 (2005).
113. Fujimoto Y., Nakatsuka M. *Jap. J. Appl. Phys*., **40**, L279 (2001).
114. Dvoyrin V.V., Mashinsky V.M., Bulatov L.I., Bufetov I.A., Shubin A.V., Melkumov M.A., Kustov E.F., Dianov E.M., Umnikov A.A., Khopin V.F., Yashkov M.V., Guryanov A.N. *Opt. Lett*., **31**, 2966 (2006).
115. Dvoyrin V.V., Kir'yanov A.V., Mashinsky V.M., Medvedkov O.I., Umnikov A.A., Guryanov A.N., Dianov E.M. *IEEE J. Quantum Electron*., **46**, 182 (2010).
116. Dianov E.M., Mel'kumov M.A., Shubin A.V., Firstov S.V., Khopin V.F., Gur'yanov A.N., Bufetov I.A. *Kvantovaya Elektron*., **39**, 1099 (2009) [*Quantum Electron*., **39**, 1099 (2009)].
117. Golant K.M., Barakutsa A.P., Butov O.V., Chamorovskij Y.K., Lanin A.V., Nikitov S.A. *ECOC 2010* (Turin, 2010) p. 1.01.
118. Gumenyuk R., Golant K., Okhotnikov O.G. *Appl. Phys. Lett*., **98**, 191108 (2011).
119. Dianov E.M., Bufetov I.A. *CLEO 2010 Techn. Dig., CMM5* (2010).
120. Chamorovskiy A., Golant K.M., Okhotnikov O.G. *Techn. Dig.37th Europ. Conf. and Exposition on Optical Commun*. (OSA, 2011) paper We.10.P1.15.
121. Chamorovskiy A., Rautiainen J., Rantamaki A., Okhotnikov O.G. *IEEE J. Quantum Electron*., **47**, 1201 (2011).
122. Chamorovskiy A., Rautiainen J., Lyytikäinen J., Ranta S., Tavast M., Sirbu A., Kapon E., Okhotnikov O. *Opt. Lett*., **35**, 3529 (2010).

123. Chamorovskiy A., Rautiainen J., Lyytikäinen J., Okhotnikov O.G. *Conf. Dig. CLEO/EQEC 2011* (Munich, 2011) p. CJ1_1.
124. Mircea A., Caliman A., Iakovlev V., Mereuta A., Suruceanu G., Berseth C.-A., Royo P., Syrbu A., Kapon E. *IEEE Photon. Technol. Lett*., **19**, 121 (2007).
125. Keller U., Weingarten K. J., Kartner F. X., Kopf D., Braun B., Jung I. D., Fluck R., Honninger C., Matuschek N., Aus der Au J. *IEEE J. Select. Top. Quantum Electron*., **2**, 435 (1996).
126. Okhotnikov O., Grudinin A., Pessa M. *New J. Phys*., **6**, 177 (2004).
127. Avdokhin A.V., Popov S.V., Taylor J.R. *Opt. Express*, **11**, 265 (2003).
128. Fermann M.E., Hartl I. *IEEE J. Select. Top. Quantum Electron*., **15**, 191 (2009).
129. http://users.ictp.it/~pub_off/preprints-sources/2009/IC2009065P.pdf.
130. Wise F.W., Chong A., Renninger W.H. *Laser & Photon.Rev.*, **2**, 58 (2008).
131. Dudley J.M., Taylor J.R. *Supercontinuum Generation in Optical Fibers* (Cambridge: Cambridge Univ. Press, 2010).
132. Lorenser D., Maas D.J.H., Unold H. ., Bellancourt A.-R., Rudin B., Gini E., Ebling D., Keller U. *IEEE J. Quantum Electron*., **42**, 838 (2006).
133. Rudin B., Wittwer V.J., Maas D.J.H.C., Hoffmann M., Sieber O.D., Barbarin Y., Golling M., Sudmeyer T., Keller U. *Opt. Express*, **18**, 27582 (2010).
134. Moloney J.V. *Proc. SPIE Int. Soc. Opt. Eng*., **5990**, 599003 (2005).
135. Morioka T., Kawanishi S., Mori K., Saruwatari M. *Electron. Lett*., **30**, 790 (1994).
136. Lindberg H., Larsson A., Strassner M. *Opt. Lett*., **30**, 2260 (2005).
137. Lindberg H., Strassner M., Gerster E., Larsson A. *Electron. Lett*., **40**, 601 (2004).
138. Lindberg H., Sadeghi M., Westlund M., Wang S., Larsson A., Strassner M., Marcinkevicius S. *Opt. Lett*., **30**, 2793 (2005).
139. Tourrenc J.P., Bouchoule S., Khadour A., Decobert J., Miard A., Harmand J.C., Oudar J.L. *Electron. Lett*., **43**, 754 (2007).
140. Symonds C., Dion J., Sagnes I., Dainese M., Strassner M., Leroy L., Oudar J.-L. *Electron. Lett*., **40**, 734 (2004).
141. Saarinen E. J., Puustinen J., Sirbu A., Mereuta A., Caliman A., Kapon E., Okhotnikov O.G. *Opt. Lett*., **34**, 3139 (2009).
142. Dupriez P., Finot C., Malinowski A., Sahu J.K., Nilsson J., Richardson D.J., Wilcox K.G., Foreman H.D., Tropper A.C. *Opt. Express*, **14**, 9611 (2006).
143. Okhotnikov O.G., Jouhti T., Konttinen J., Karirinne S., Pessa M. *Opt. Lett*., **28**, 364 (2003).
144. Saarinen E.J., Härkönen A., Herda R., Suomalainen S., Orsila L., Hakulinen T., Guina M., Okhotnikov O.G. *Opt. Express*, **15**, 955 (2007).
145. Chamorovskiy A., Kerttula J., Rautiainen J., Okhotnikov O.G. *Electron. Lett*., **48**, 1010 (2012).